A&A 466, 421–435 (2007)
DOI: 10.1051/0004-6361:20065405

Astronomy & Astrophysics

Structure and evolution of magnetized clusters: entropy profiles, $S - T$ and $L_X - T$ relations

S. Colafrancesco and F. Giordano

INAF - Osservatorio Astronomico di Roma, via Frascati 33, 00040 Monteporzio, Italy
e-mail: cola@mporzio.astro.it

Received 10 April 2006 / Accepted 21 December 2006

ABSTRACT

We study the impact of an intracluster magnetic field on the main structural properties of clusters and groups of galaxies: the radial density and entropy profiles, the entropy – temperature relation and the X-ray luminosity – temperature relation for groups and clusters of galaxies. To this aim, we develop a description of the intra-cluster gas based on the Hydrostatic Equilibrium condition and on the Magnetic Virial Theorem in the presence of a radial distribution of the magnetic field $B(r) = B_*(\rho_g(r))^\alpha$, with $\alpha \approx 0.9$, as the one indicated by observations and numerical simulation. Our analysis shows that such a description is able to provide, at once, a possible explanation of three problematic aspects of the cluster structure: i) the flattening of the entropy profile in the cluster center; ii) the flatness of the $S - T$ relation; iii) the increasing steepening of the $L_X - T$ relation from the cluster scale towards the group scales. The available entropy and X-ray luminosity data indicate that an increase of the magnetic field $B_* \sim T^{0.5\pm0.1}$ is required to reproduce at the same time both the $S - T$ and the $L_X - T$ relations. It follows that a consistent description of the magnetized ICM can provide a simple explanation of several (or of all) of these still open problems, and thus weakens the need for the inclusion of other non-gravitational effects which have been proposed so far for the explanation of some of these features. This (initial, but not conclusive) analysis can be regarded as a starting point for a more refined analytical exploration of the physics of the magnetized intra-cluster medium, and it provides testable predictions that can be proven or disproven with the next coming sensitive observations of groups and clusters in the X-ray band and in the radio frequency band.

Key words. cosmology: theory – galaxies: clusters: general

1. Introduction

It has been well known since the early 1990s that the intra-cluster (IC) gas properties deviate from the self-similar predictions of the standard CDM model. The first and most noticeable piece of evidence is provided by the fact that the X-ray luminosity (L_X) – temperature (T) relation is steeper than expected from a standard ΛCDM model (see, e.g., Arnaud & Evrard 1999; Mushotzky 2003; Arnaud 2005, for a review). This evidence indicated the need for a more detailed look at the IC gas properties. As a result, the idea that non-gravitational processes can play indeed a role in determining the cluster structure and evolution has been widely accepted (Evrard & Henry 1991; Ponman et al. 2003; see Arnaud 2005, for a review). The picture obtained by the high-sensitivity, high-throughput X-ray telescopes (Chandra, XMM-Newton) provided a wealth of precise information on several aspects of the structure and evolution of clusters and groups of galaxies.

The local relations of various physical quantities (i.e., temperature, entropy, X-ray luminosity, mass) to the temperature of the IC gas (i.e., a measure of their potential wells and of their equilibrium stage) show that the global IC gas properties like the X-ray luminosity L_X (Markevitch 1998; Arnaud & Evrard 1999), the IC gas mass M_{gas} (e.g., Mohr et al. 1999) or the gas mass fraction $f_g \equiv M_{gas}/M$ scale with the IC gas temperature T differently than expected from pure gravitational self-similar evolution of these systems (see Arnaud 2005, for a review). It has been suggested that the departures of the IC gas scaling laws from the standard self-similar model are likely due to a non-standard scaling of the mean gas density with temperature and not to a break of the self-similarity (see Arnaud 2005, for a general discussion). The gas entropy, defined as $S = k_B T_g/\rho_g^{2/3}$ and related to the true thermodynamic entropy via a logarithm and an additive constant, is considered in this context as a fundamental quantity describing the IC gas and therefore can greatly help to understand the thermodynamic history of the IC gas (e.g., Voit et al. 2002; Voit 2005). In the standard CDM self-similar scenario, the entropy should scale simply as $S \propto T$ at any scaled radius. However, it is known that the entropy measured at a radius $r = 0.1r_{200}$ exceeds the value predicted by the pure gravitation-based model (Pratt & Arnaud 2003; Pratt et al. 2006; Donahue et al. 2006; Piffaretti et al. 2005), an effect that is especially strong for low-T clusters (Ponman et al. 1999, 2003). Various non-gravitational processes have been proposed to explain this entropy excess, such as heating (from SNs and/or AGNs) before or after the cluster collapse, or radiative cooling (see, e.g., Voit 2005, for a review), but none of these is able to provide a conclusive explanation of this problem.

In this framework, recent XMM data (e.g., Pratt & Arnaud 2003; Pratt et al. 2006) show a remarkable self-similarity in the entropy radial profiles for clusters with $k_B T \gtrsim 2$ keV, a result which is also consistent with a stacking analysis of ROSAT data (Ponman et al. 2003). The self-similarity of the radial shape of cluster entropy profiles proves to be a strong constraint for cluster models. For instance, simple pre-heating models, which predict large isentropic cores, should be ruled out (Arnaud 2005). Furthermore, the slope of the entropy profiles seems to be slightly shallower than predicted by shock-heating models (Arnaud 2005). A complex interplay of gravitational,

cooling and galaxy feedback mechanisms is usually considered in the attempt to provide a consistent picture (see, e.g., Voit 2005, for a review). It is clear that an unambiguous description of the structure and evolution of groups and clusters can be obtained only by studying in detail the internal structure of these systems (see, e.g., Arnaud 2005).

In this context, there has been no attempt, so far, to incorporate a detailed description of the effect of magnetic fields on the IC gas distribution, irrespective of the fact that there are several unambiguous and independent pieces of evidence for the presence of magnetic fields at the $\gtrsim\mu$G level, especially in the inner regions of galaxy clusters and groups (see, e.g., Carilli & Taylor 2002; Govoni & Feretti 2005) as well as several numerical (see, e.g., Dolag et al. 2001) and theoretical motivations (see, e.g., Colafrancesco et al. 2005; see also Giovannini 2004, for a review) for its presence and extended spatial distribution.

In this paper we will explore the role of the magnetic field B in determining the structural properties of virialized groups and clusters. We will first show in Sect. 2 the effect of the magnetic field in determining the properties of the IC gas in hydrostatic equilibrium (HE) and their thermal structure from the Magnetic Virial Theorem (MVT). We will discuss in Sect. 3 the entropy profiles of magnetized clusters. In Sect. 4 we will discuss the cluster basic $M - T$ relation and we will show in Sect. 5 that the inclusion of the B-field provides a flattening of the $S - T$ relation, by acting on the IC gas thermal and density properties. We will then apply our considerations to the $L_X - T$ relation in Sect. 6 and show that the inclusion of the B-field that reproduce the $S - T$ relation also recovers the observed steepening of the $L_X - T$ relation, from rich cluster to poor groups. A systematic exploration of the role of the IC gas boundary conditions on the density, entropy and X-ray luminosity scaling with the cluster temperature will be provided in Sect. 7. We will finally discuss our results in Sect. 8 in the context of the existing experimental and theoretical framework, and we will present our basic conclusions. The relevant physical quantities are calculated using $H_0 = 71$ km s^{-1} Mpc^{-1} and a flat, vacuum-dominated CDM ($\Omega_m = 0.3, \Omega_\Lambda = 0.7$) cosmological model.

2. The structure of magnetized clusters

We derive in this section the relevant quantities that describe the cluster structure in the presence of a magnetic field. These are the density and the temperature of the IC gas, both depending, in general, on the magnetic field.

2.1. Hydrostatic equilibrium of the ICM in the presence of magnetic field

The gravitational potential of a galaxy cluster is determined mainly from the DM distribution which contributes more that ∼90% of its total mass. We assume here, for simplicity, that the DM density profile is described by the NFW profile (Navarro et al. 1997)

$$\rho_{dm} = \rho_s y_{dm}(x) = \rho_s \frac{1}{x(1+x)^2}, \quad (1)$$

where $x \equiv r/r_s$, r_s is the scale radius, ρ_s is a normalization factor and $y_{dm}(x)$ describes the radial density profile of the DM in terms of the adimensional radius x. The scale radius r_s is linked to the virial radius r_{vir} by means of the concentration parameter $c \equiv r_{vir}/r_s$, where

$$r_{vir} \equiv [M_{vir}/(4\pi\Delta_c(z)\rho_c(z)/3]^{1/3}, \quad (2)$$

and $\rho_c(z)$ is the cosmological closure density at redshift z. The quantity $\Delta_c(z)$ is the average density of the DM halo with total mass $M_{vir} \equiv M(\leq r_{vir})$ in units of the critical density at redshift $z = 0$ and takes the value $\Delta_c \sim 100$ in the reference cosmological model we consider here ($\Omega_m = 0.3$, $\Omega_\Lambda = 0.7$). We adopt here the predicted value of $\Delta_c(z)$ from Eke et al. (1996). The concentration parameter c scales mildly with the cluster mass as

$$c = 6\left(\frac{M_{vir}}{10^{14}\, h^{-1} M_\odot}\right)^{-0.2} \quad (3)$$

(see Seljak 2000; Colafrancesco et al. 2006). Given the previous DM halo structure, the gas density ρ_g and its temperature T can be obtained from the hydrostatic equilibrium (HE) condition once the equation of state for the gas is specified. The three cases usually considered are: i) the gas follows the DM, $\rho_g \propto \rho_{dm}$ (see, e.g., Wu & Xue 2002); ii) the isothermal case $T_g = $ const. (see, e.g., Komatsu & Seljak 2001); iii) the polytropic case, $T_g \propto \rho_g^{\gamma-1}$ (see, e.g., Komatsu & Seljak 2001; Zhang 2004). We concentrate here on the isothermal case and we improve it by including the effects of the magnetic field.

The condition of hydrostatic equilibrium (HE) in the presence of a magnetic field $B(r)$ can be written as

$$\frac{dP_g}{dr} + \frac{dP_B}{dr} = -\frac{GM(\leq r)}{r^2}\rho_g, \quad (4)$$

where $\rho_g \equiv \rho_g(r, B)$ is the density of the thermal diffuse IC gas and $P_g \equiv P_g(r, B)$ is its pressure, with both quantities depending in general on the magnetic field B. The magnetic field pressure, $P_B \propto B^2(r)$, adds to the left hand term of Eq. (4). The magnetic pressure determines, hence, the final distribution of the IC gas density $\rho_g(r, B)$ since it tends to counterbalance part of the gravitational pull of the cluster thus prohibiting the gas from a further infalling that results in a less concentrated gas core.

We assume, in the following, a parametric form of the magnetic field radial distribution

$$B(r) = B_*\left(\frac{\rho_g(r)}{10^4\bar{\rho}_g(z=0)}\right)^\alpha, \quad (5)$$

where $\rho_g(r)$ is the solution of the HE equation (see Appendix A), $\bar{\rho}_g(z = 0)$ is the average cosmological density of the gas at $z = 0$, B_* is measured in μG and α is a parameter $\geq 2/3$ (see, e.g., Zhang 2004; Carilli & Taylor 2002; Dolag et al. 2001). We assume in our calculations here a value $\alpha = 0.9$ as indicated by numerical simulations (e.g., Dolag et al. 2001).

In the Appendix A we have derived the solution of the HE equation in the presence of a magnetic field $B(r)$ for two cases of the equation of state of the IC gas: i) the isothermal case; and ii) the polytropic case.

We discuss here specifically the IC gas distribution in the case of a isothermal condition in which the Magnetic Virial Theorem (MVT) derived for galaxy clusters by Colafrancesco & Giordano (2006) also holds. We will address the polytropic case and more general cases with a radial dependence of the cluster temperature elsewhere (Colafrancesco & Giordano 2007, in preparation).

Under these assumptions, we derived numerically the solution of the HE equation for the IC gas density $\rho_g(r, B)$. Figure 1 shows the density profile of the IC gas derived from the HE condition and normalized to the cluster gas mass evaluated at the virial radius as a function of the radius for different values of the magnetic field B_*. The effect of the magnetic field is shown for various masses of the cluster $M = 0.5, 1$ and $5\ M_8$,

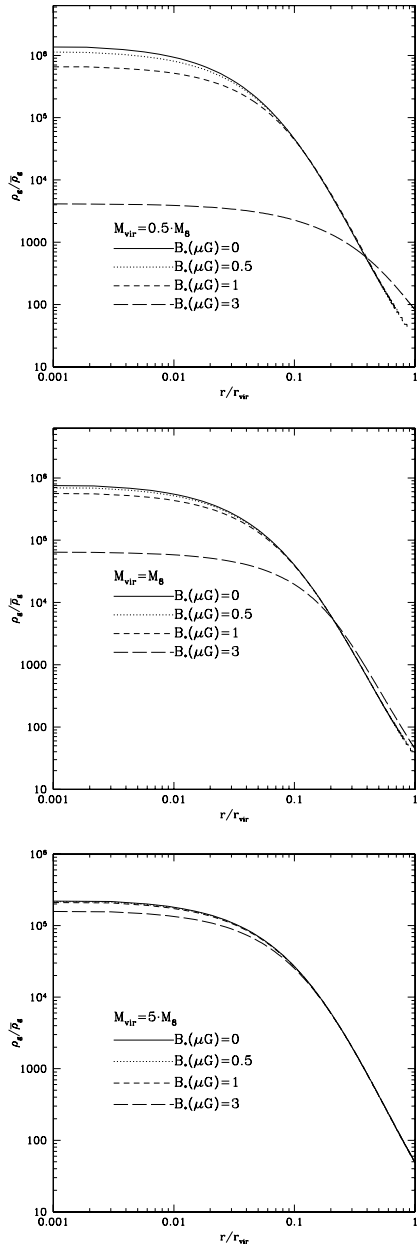

Fig. 1. The IC gas density profile as derived from Eqs. (A.19)–(A.20) for three different cluster masses (as labelled in the three panels), and for values of the magnetic field $B_* = 0$ (solid), 0.5 (dotted), 1 (short dashes) and 3 (long dashes) μG. The density profiles are normalized to the total gas mass at $r_{\rm vir}$.

where M_8 is the mass enclosed in a 8 h^{-1} Mpc radius spherical fluctuation at the epoch at which it goes non-linear: it takes the value $M_8 \approx 2 \times 10^{14}\ h_{71}^{-1}\ M_\odot$ in our reference cosmological model. The B-field provides a pressure that tends to inflate the IC gas so that its final radial profile extends outwards, in the case of density normalized to the central IC gas density in the absence of the B-field. Since observations and our modelling of the cluster structure provide a measure of the gas distribution for a given mass (within a fixed radius), we study the effect of the B-field for a fixed gas mass, i.e., extended, say, up to the virial radius, or more generally to the radius r_Δ at which the density contrast is Δ (see the Appendix for details). Thus, the requirement to recover the fixed gas mass at the virial radius yields the relation

$$\rho_{\rm g}(r, B) = K(M, B) \cdot \rho_{\rm g}(r, B = 0), \qquad (6)$$

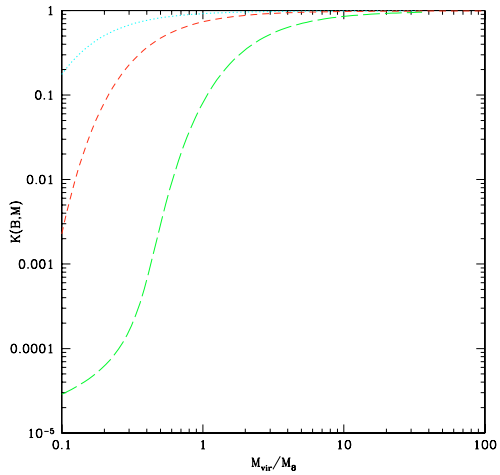

Fig. 2. The function $K(M, B) = \rho_{\rm g}(r, B)/\rho_{\rm g}(r, B = 0)$, evaluated at $r = 0.1 r_{200}$, is shown as a function of the cluster mass and for three different values of the magnetic field $B_* = 0.5$ (cyan), 1 (red) and 3 (green) μG.

with

$$K(M, B) = \frac{\int_0^c {\rm d}x x^2 y_{\rm g}(x, 0)}{\int_0^c {\rm d}x x^2 y_{\rm g}(x, B)}. \qquad (7)$$

Such boundary conditions provide a decrease of the central gas density for increasing values of B_* (see Fig. 1). The effect of $B(r)$ clearly becomes milder for more massive systems due to the large DM and gas mass contained there. In fact, the normalization function $K(M, B) = \rho_{\rm g}(r, B)/\rho_{\rm g}(r, B = 0)$ steeply rises from its low value at low masses and rapidly reaches unity at mass scales that increase with increasing values of B_* (see Fig. 2). Larger values of B_*, hence, increase the cluster mass range that is sensitive to the effect of the magnetic field.

The ratio of the magnetic to IC gas pressure, $P_B/P_{\rm g}$, corresponding to the density profiles shown in Fig. 1 are calculated at three different radii $r = 0$, $0.1 r_{200}$ and r_{200} and are shown in Fig. 3 as a function of the cluster temperature. The ratio between the magnetic pressure, $P_B \propto 8\pi B^2(r)$, and the IC gas pressure, $P_G \propto \rho_{\rm g} T_{\rm g}$, scales as $P_B/P_{\rm g} \propto B_*^2 \rho_{\rm g}^{2\alpha-1}/T_{\rm g} \sim B_*^2 K^{2\alpha-1}/T_{\rm g}$ according to our assumption for $B(r)$ (see Eq. (5)). For relatively high masses, when the function $K = \rho_{\rm g}(r, B)/\rho_{\rm g}(r, B = 0) \to 1$ (see Fig. 2), the pressure ratio $P_B/P_{\rm g} \propto B_*^2 T_{\rm g}^{-1}$ and its amplitude scales with the value of B_*^2. For low masses the gas density is strongly affected by the magnetic field and hence the function K strongly decreases with decreasing M so that the pressure ratio decreases with decreasing M (or T) as $P_B/P_{\rm g} \propto K^{2\alpha-1} T^{-1}$ At an intermediate mass (temperature) between the low-T tail (where $P_B/P_{\rm g}$ strongly decreases) and high-T tail (where $P_B/P_{\rm g}$ asymptotically decreases as $1/T_{\rm g}$), the pressure ratio attains its maximum (following the curvature of the function K). The temperature (mass) location of the maximum of $P_B/P_{\rm g}$ depends of the value of B_* reflecting the behaviour of the function K as a function of B_*, i.e. the behaviour of the gas density profiles shown in Fig. 1. In our specific model for the density and temperature of the IC gas in the presence of a magnetic field, the value $P_B/P_{\rm g}$ is ~25% at most and peaks at increasing values of T for increasing amplitude of B_*. The specific values of the maximum of $P_B/P_{\rm g}$, of its temperature (mass) location and of the low-T tail depend on the specific choice for the exponent α in Eq. (5) and are not universal. Nonetheless, the general trend of the pressure ratio shown in Fig. 3 is preserved for the specific

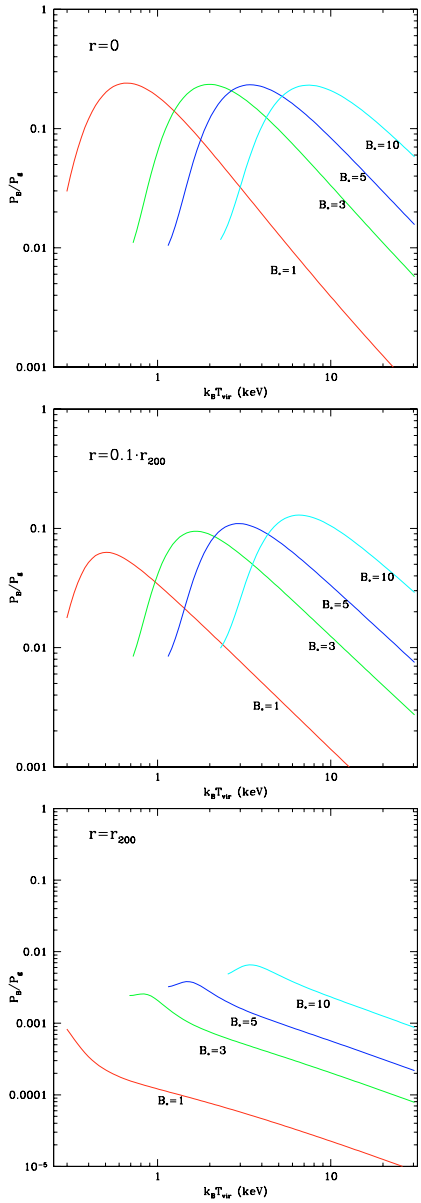

Fig. 3. We show the ratio P_B/P_g between the IC gas pressure and the magnetic pressure as a function of the cluster temperature for different values of the magnetic field $B_* = 1$ (red), 3 (green), 5 (blue) and 10 (cyan) μG. The ratio P_B/P_g is shown at three different cluster radii: $r = 0$ (*upper panel*), $r = 0.1r_{200}$ (*mid panel*) and $r = r_{200}$ (*lower panel*).

form of the radial dependence of the magnetic field as in Eq. (5) and for values of $\alpha > 0.5$, as indicated by the available data.

2.2. The magnetic virial theorem for galaxy clusters

The temperature of the IC gas that is used in the HE condition is consistently derived, in the framework of our isothermal model, from the magnetic virial theorem (MVT). We recall here the main aspects of the IC gas temperature derivation from the MVT following Colafrancesco & Giordano (2006).

Under the assumption of an ICM in hydrostatic equilibrium with the potential well of a spherically-symmetric, isolated, virialized and magnetized cluster, the general relation between the ICM temperature T_g and the cluster virial mass M_{vir} is obtained by applying the MVT that, for a static and isothermal galaxy cluster, reads

$$2K + 2U + U_B + W = 0. \tag{8}$$

Here U_B is the magnetic energy of the system, U is the kinetic energy of the gas (we assume that the Dark Matter is cold and collisionless), K is the Dark-Matter particle kinetic energy and W is the total potential energy (see Colafrancesco & Giordano 2006, for details). The previous Eq. (8) holds specifically in the absence of an external medium. For the more general case of a cluster that is immersed in a Inter Galactic Medium (IGM) or in an external medium that exerts an external pressure P_{ext}, Eq. (8) yields the formula for the temperature of the gas in virial equilibrium

$$\frac{k_B T_g}{\mu m_p} = \frac{\xi G}{3}\frac{M_{vir}}{r_{vir}}\left(1 - \frac{M_\phi^2}{M_{vir}^2} + \frac{P_{ext}}{P_{vir}}\right), \tag{9}$$

where $P_{vir} = (\frac{4\pi}{\xi G}\frac{r_{vir}^4}{M_{vir}^2})^{-1}$ with usually $\xi \gtrsim 1$, and M_ϕ is given by

$$M_\phi \simeq 1.32\times 10^{13} M_\odot \left[\frac{I(c)}{c^3}\right]^{1/2}\left(\frac{B_*}{\mu G}\right)\left(\frac{r_{vir}}{\mathrm{Mpc}}\right)^2. \tag{10}$$

Here $I(c) = \int_0^c (\rho_g(r=0)/\bar\rho_g(z=0))^{2\alpha} x^2 y_g^{2\alpha}(x, B=0)\mathrm{d}x$, and $y_g(x, B=0) = \rho_g(x)/\rho_g(x=0)$ is the gas density profile normalized to the central gas density (i.e. the solution of the hydrostatic equilibrium equation in the absence of a magnetic field, see Appendix for details).

For the case $P_{ext} = 0$ and $B = 0$, one finds $M_\phi = 0$ and the well-known relation

$$k_B T_g(B=0) = -\frac{\xi \mu m_p W}{3 M_{vir}} \tag{11}$$

re-obtains (here $\mu = 0.63$ is the mean molecular weight, corresponding to a hydrogen mass fraction of 0.69, m_p is the proton mass and k_B is the Boltzmann constant).

For $B > 0$, one finds $M_\phi > 0$ and the temperature of the gas at fixed M_{vir} reads

$$kT_g = kT_g(B=0)\left(1 - \frac{M_\phi^2}{M_{vir}^2} + \frac{P_{ext}}{P_{vir}}\right). \tag{12}$$

The temperature of a cluster calculated in the presence of a magnetic field (with $P_{ext} = 0$) is lower than that given by Eq. (11) because the additional magnetic field energy term U_B adds to the MVT.

The presence of an external pressure P_{ext} tends to compensate the decrease of T_g induced by the magnetic field. In the following, we consider values of P_{ext} (which are relevant for the structures we consider here) as estimated in the IGM and in the rich cluster outskirts. For values of the temperature, $T_{IGM} \sim 10^6$ K, and density, $n_{IGM} \sim 10^{-5}$ cm^{-3}, as estimated by the WHIM structure around large-scale overdensities (see, e.g., Fang & Bryan 2001), $P_{ext} \sim 1.7 \times 10^{-3}$ eV cm$^{-3}(n_{IGM}/10^{-5}$ cm$^{-3})(T_{IGM}/2\times 10^6$ K). However, in the outer regions of massive clusters (at $r \gtrsim r_{vir}$, where the main source of pressure could be due to the momentum of the infalling gas accreting onto the cluster), studies of the mean projected temperature profile for the cluster sample derived by Piffaretti et al. (2005, see their Fig. 4) indicate that the external gas pressure can reach values up to $P_{ext} \sim 0.2$ eV cm$^{-3}(n/10^{-4}$ cm$^{-3})(T_g/1.7\times 10^7$ K) (we consider here a typical rich cluster with $T_g = 10$ keV). In the case of such

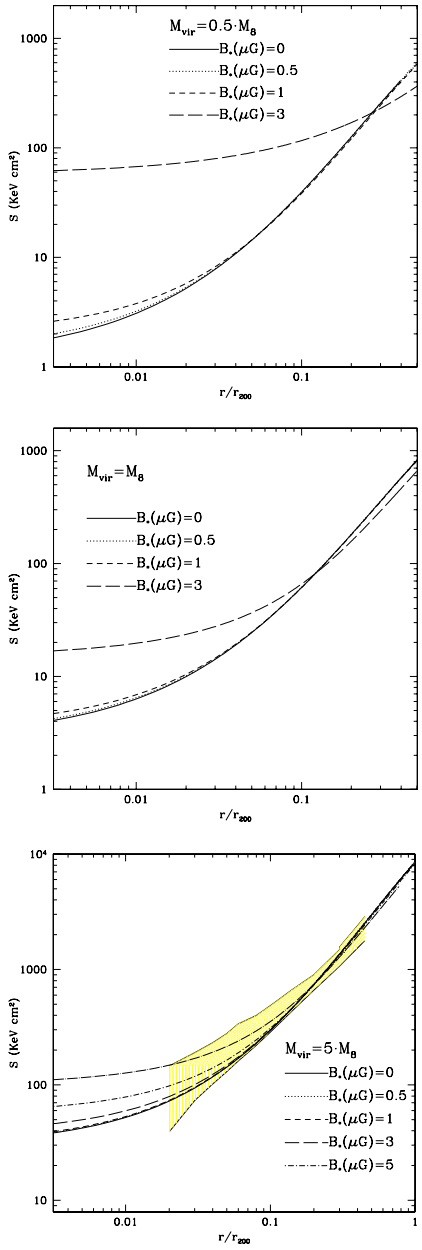

Fig. 4. IC gas entropy profile for various values of the magnetic field $B_* = 0, 0.5, 1$ and 3 μG and for three different cluster masses: $0.5M_8$ (*top panel*), M_8 (*mid panel*) and $5M_8$ (*bottom panel*). The density profiles are normalized to the total gas mass at $r_{\rm vir}$. The shaded region in the last plot for a cluster with $M_{\rm vir} = 5M_8$ show the 1 sigma area spanned by the normalized entropy profiles derived by Pratt et al. (2006) for 10 nearby clusters.

a hot cluster, the value of $P_{\rm ext}$ is a significant fraction, ∼4%, of the central ICM pressure and ∼50% of the ICM pressure at the virial radius for a typical cluster. However, for lower-temperature clusters, such values of $P_{\rm ext}$ are expected to be sensitively lower. A value $P_{\rm ext} \sim 0.2$ eV cm^{-3}, as estimated at the outskirts ($r \gtrsim r_{\rm vir}$) of rich, hot clusters, can be considered, hence, as an upper bound to $P_{\rm ext}$; in addition, an exact determination of the total cluster mass (which is subject to various systematic uncertainties, see, e.g., Rasia et al. 2006) requires an extension beyond $r_{\rm vir}$. Lower values of $P_{\rm ext}$, down to the value found in the WHIM, have progressively less importance for the MVT.

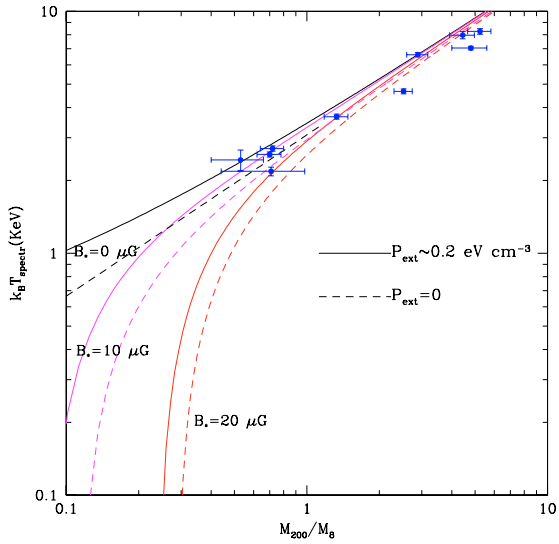

Fig. 5. The $T_{\rm spectr} - M_{200}$ relation at $z = 0$ for clusters that contain a magnetic field $B_* = 0$ (black), 10 (magenta) and 30 μG (red), and for values of $P_{\rm ext} = 0$ (dashed curves) and $P_{\rm ext} = 0.2$ eV cm^{-3} (solid curves). Data are taken from Arnaud (2005).

For reasonable values of $B_* \gtrsim$ a few μG, the quantity $M_\phi^2 > M_{\rm vir}^2 \cdot (P_{\rm ext}/P_{\rm vir})$ in Eq. (9) and the main effect is a reduction of the cluster temperature which is more pronounced for less massive systems, where M_ϕ becomes comparable to $M_{\rm vir}$. The effects of the magnetic field and of the external pressure are greater for low-M clusters (see Colafrancesco & Giordano 2006, and Fig. 5).

3. The radial entropy profiles of magnetized clusters

Given the previous results on the temperature and on the gas density in the presence of a B-field, we can now discuss the impact of the magnetic field on the entropy profile of galaxy clusters.

The entropy of the IC gas is usually defined as

$$S = \frac{k_{\rm B} T_{\rm g}}{\rho_{\rm g}^{2/3}} \tag{13}$$

and, in our model, it depends on the magnetic field through the B-dependence of the cluster temperature $T_{\rm g}(B)$, as derived from the MVT (see Eq. (8)), and from the IC gas density $\rho_{\rm g}(r, B)$, as derived from the HE condition (see Eqs. (A.19)–(A.20)).

Our model provides a simple but consistent description of the B-dependence of the (isothermal) cluster entropy and contains all the relevant physical information. However, the detailed effect of the magnetic field on the cluster entropy should be addressed in a truly magneto-hydro-dynamical (MHD) model of cluster formation and evolution, which is able to catch the details of the turbulent amplification and of the evolution of the B-field associated with the shocked gas in the cluster environment. Such a task is well beyond the scope of this paper and could be better tackled through MHD cosmological simulations and/or semi-analytical methods that will be addressed elsewhere. Nonetheless, the model we present here is able to describe the overall properties of cluster entropy, namely its radial behaviour and its correlation with the cluster temperature. In Fig. 4 we show the radial entropy profiles of the IC gas calculated by using the IC gas density profiles normalized to the cluster mass gas

(these are shown in Fig. 1). The entropy profiles we obtain flatten in the inner cluster region for increasing values of the magnetic field B_*. This behaviour reflects the decrease of the central IC gas density for increasing values of the magnetic field, as shown in Fig. 1. The bottom panel in Fig. 4 shows also the comparison of our entropy profiles for a typical $M_{\rm vir} = 5M_8$ cluster with the region enclosed by the mean plus/minus the 1σ standard deviation of the scaled entropy profiles for ten clusters observed with XMM (Pratt et al. 2006). These clusters have, in fact, quite high masses around the reference value we consider here. The predictions of our model agree quite well with the data, and the widening of the observed entropy profiles at small radii could reflect the dispersion of the B-dependent density profiles found for high values of B_*. In this respect, the XMM cluster data, taken at face value, limit the amplitude of the magnetic field to values $B_* \lesssim 7\ \mu$G for this mass range.

The mean temperature used to investigate the scaling properties of the XMM clusters has been estimated in the region $0.1r_{200} < r < 0.5r_{200}$ and it is quite constant for most of the XMM clusters (see Pointecouteau et al. 2005). This fact allows us to directly compare the predictions of our isothermal model with the observed entropy profiles derived by Pratt et al. (2006).

Furthermore, our model predicts a sensitive flattening of $S(r)$ at smaller radii $<0.2r_{200}$ which is more evident for higher values of B_*. This behaviour is similar to the entropy flattening shown in the inner cool cores of the clusters studied with Chandra (see, e.g., Donahue et al. 2006). Note, however, that a closer comparison of the (isothermal) model we consider here with these cool cluster cores (where one observes temperature jumps of the order of a factor of 2–3 with respect to the outer temperature, see, e.g., Colafrancesco et al. 2004, and references therein) cannot be done straightforwardly, and it demands a more detailed modeling of the magnetized core regions that will be presented elsewhere (Colafrancesco & Giordano 2007, in preparation).

4. The $M - T$ relation for magnetized clusters

To derive consistent structural relationships for clusters and groups, we first need to derive their $M-T$ relation. The $M-T$ relation is a basic structural relation for groups and clusters and it is the starting point to study the entropy and X-ray luminosity scaling with T and/or M. The $T - M$ relation for magnetized clusters has been derived by Colafrancesco & Giordano (2006) and is also shown in Fig. 5 where it is compared to the data for the XMM clusters used to derive the entropy profiles previously discussed (see Pratt et al. 2003). Our isothermal model is consistent with the previous data because these are obtained by using an overall spectroscopic temperature (which is constant in the radial range $(0.1–0.5)r_{200}$ and also because the values of $T_{\rm spectr.}$ have been obtained by performing an isothermal fit of the cluster spectra obtained in the same $(0.1–0.5)r_{200}$ radial range.

The normalization of the observed $T_{\rm spectr.} - M_{200}$ relation is however found to be discrepant by ∼30% with respect to the value derived from numerical simulations including only gravitational heating (see, e.g. Evrard et al. 1996), a well known problem (see, e.g., Arnaud 2005, for a review) which usually requires one to re-normalize the predictions of analytical models. In our model we normalize the $T_{\rm spectr.} - M_{200}$ relation for the case $B = 0$ to the observed data derived by Arnaud et al. (2005) by assuming $T_{\rm spectr} = T_{\rm g}$, where $T_{\rm g}$ is obtained from Eq. (9), and a temperature boost of a factor $\xi \approx 1.5$ in Eq. (9), as can be expected from the continuous shock-heating of the IC gas within the virial radius after the formation of the original structure (see, e.g., Makino et al. 1998; Fujita et al. 2003; Ryu et al. 2003). Such a prescription for ξ has been used by the previous authors for unmagnetized clusters in the absence of external pressure. A systematic effect which tends to increase the cluster temperatures is the presence of a minimal external pressure in Eqs. (9) and (12). A value $P_{\rm ext} \sim (0.1–0.2)P_{\rm vir}$ (like that found in the IGM around clusters) could easily accommodate for an overall boost value of $\xi \approx 1.5 \times (P_{\rm ext}/P_{\rm vir}) > 1.5$ and reasonably in the range 1.65–1.8, for the previous values of $P_{\rm ext}$. Given the large theoretical uncertainty on the non-gravitational heating efficiency, we adopted an overall value $\xi \approx 1.8$ to normalize our prediction to the data point at $M_{200} \approx 3 \cdot M_8$ in Fig. 5, which is the point with the smaller intrinsic error. However, values of ξ in the plausible range 1.5–1.8 marginally change our predictions.

The relation $M_{200} \simeq 0.77 M_{\rm vir}$ is also found in our mass scale definition.

Small variations of temperatures with respect to their unmagnetized values are found for massive clusters since $M_\phi \ll M_{\rm vir}$ in this mass range and the value of $P_{\rm ext}$ has little or negligible effect (see Fig. 5). This is in agreement with the results of numerical simulations (Dolag et al. 2001a). However, when M_ϕ becomes comparable to $M_{\rm vir}$, the IC gas temperature becomes lower than its unmagnetized value and the $T - M$ relation steepens in the range of less massive systems like groups and poor clusters. The temperature $T_{\rm g}$ formally tends to zero when $M_\phi \to M_{\rm vir}(1 + P_{\rm ext}/P_{\rm vir})^{1/2}$. However, this limit is unphysical since it corresponds to an unstable system in which the magnetic pressure overcomes the gravitational pull. Thus, any physical configuration of magnetized virialized structures must have $M_\phi < M_{\rm vir}(1 + P_{\rm ext}/P_{\rm vir})^{1/2}$.

The effect of $P_{\rm ext}$ counterbalances the effect of the B-field on the $T - M$ relation, and its amplitude increases for low-M systems. (see Fig. 5; see also Colafrancesco & Giordano 2006, for details).

5. The $S - T$ relation for magnetized clusters

Using the $T - M$ relation presented in Sect. 4, we can now derive our predictions for the $S - T$ relation for clusters with a magnetic field. Here, we will compare our models for the IC gas distribution in the presence of a magnetic field with the data of the $S - T$ relation (see Ponman et al. 2003; see also Arnaud 2005, for a review). The entropy in this correlation has been evaluated at a distance $0.1r_{200}$ from the cluster center and thus we have to evaluate both the IC gas density and its temperature at this radius.

Due to the decrease of the IC gas density for increasing values of the magnetic field (see Fig. 1), the density of the IC gas evaluated at a distance $0.1r_{200}$ exhibits a peculiar trend with increasing cluster temperature (mass) as shown in Fig. 6. The presence of a temperature dependence of the gas density $\rho_{\rm g}(0.1r_{200})$, even in the case $B = 0$, is a consequence of the HE condition (see Eq. (4)), independently of the chosen equation of state for the gas in the MVT. The specific solution of the HE condition for the unmagnetized case ($B = 0$) is given in Eq. (A.10) of the Appendix. It is clear that $\rho_{\rm g}(r) \propto \exp[-3c/m(c) \int_0^x {\rm d}um(u)/u^2]$ exhibits a temperature dependence (like that shown in Fig. 6) since the concentration parameter c depends on $T_{\rm g}$ through Eq. (3).

For each fixed value of B_*, the presence of a B-field produces a sharp rise of the gas density $\rho_{\rm g}(0.1r_{200})$ in the low-T region followed by a smooth decline at higher temperatures where the density tends to the unmagnetized value (solid black curve). This effect is produced by the physical boundary condition for the IC gas density, i.e. by the requirement to normalize the IC gas

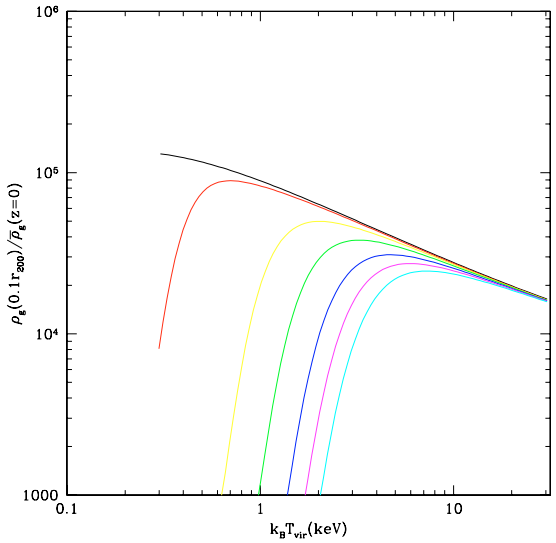

Fig. 6. The temperature dependence of the IC gas density evaluated at $0.1r_{200}$ for various values of the magnetic field $B_* = 0$ (black curve), 0.5 μG (red), 1 μG (yellow), 2 μG (green), 3 μG (blue), 5 μG (magenta) and 10 μG (cyan).

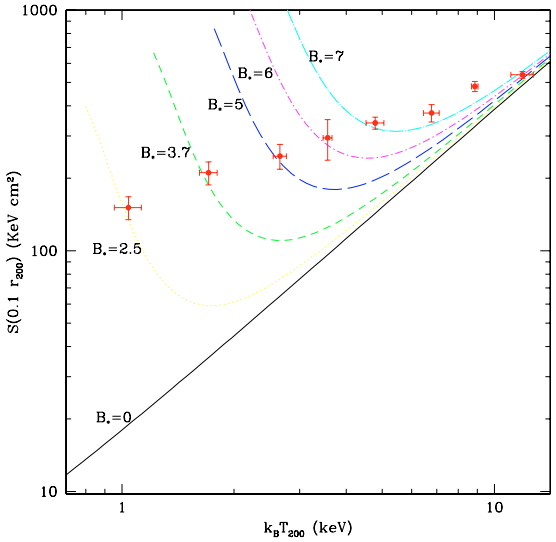

Fig. 7. The entropy $S(0.1r_{200})$ as a function of the temperature for various values of the magnetic field B_* as labelled. The binned entropy data are taken from Ponman et al. (2003).

density to the total gas mass at $r_{\rm vir}$ for each cluster. The sharp rise of $\rho_{\rm g}(0.1r_{200})$ with the cluster temperature (mass) is produced by the effect of the function $K(M, B)$ (see Fig. 2): when $K \to 1$ at high masses, then $\rho_{\rm g}(0.1r_{200}, B)$ tends to its value for unmagnetized clusters with $B = 0$ (i.e., the black curve in Fig. 6, see also discussion in Sect. 2.1).

Given the temperature behaviour of $\rho_{\rm g}(0.1r_{200})$ and the value of the IC gas temperature at the same radius, the $S - T$ relation for magnetized clusters predicted by our model can be calculated using Eq. (13) and is shown in Fig. 7. We stress that, based on the HE condition for the IC gas, one has to expect an entropy scaling with the gas temperature which is different from the one, $S \sim T$, usually associated with "standard self-similar" models, even in the case $B = 0$; the actual scaling is, in particular, steeper than $S \sim T$ due to the decreasing behaviour of $\rho_{\rm g}(0.1r_{200})$ with increasing T (see Fig. 6).

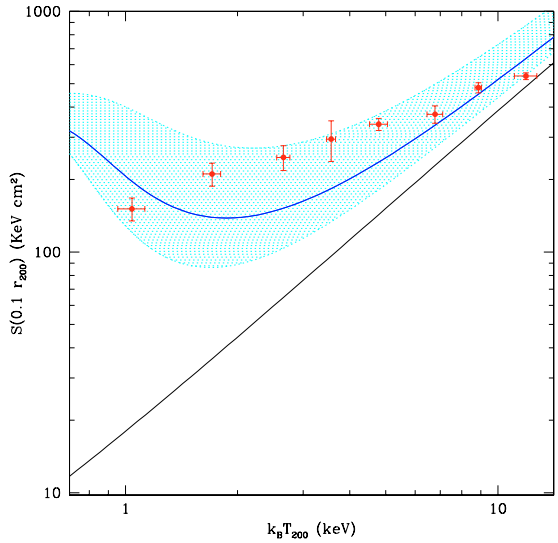

Fig. 8. The entropy $S(0.1r_{200})$ is shown as a function of the temperature for a magnetic field scaling $B_* \sim T_{200}^{\eta}$ with $\eta = 0.5$ (solid curve). The dashed area enclosed by the two entropy curves calculated for $B_* \sim T_{200}^{0.4}$ and for $B_* \sim T_{200}^{0.6}$ shows the range of variation for B_* allowed by the binned entropy data.

The effect of a fixed amplitude of the magnetic field B_* (set constant here for any cluster) is to flatten the $S - T$ relation due to the combination of the decrease in $T_{\rm g}$ caused by the MVT and to the decrease of the IC gas density $\rho_{\rm g}(0.1r_{200})$ caused by the HE condition. The entropy inversion shown for low-T (at fixed value of B_*) in Fig. 7 reflects the sharp cutoff at low-T in the gas density $\rho_{\rm g}(0.1r_{200})$ shown in Fig. 6. The binned entropy data derived from Ponman et al. (2003) shown in Fig. 7 are enclosed by the two curves for $B_* = 2.5$ and 7 μG. This indicates that a magnetic field whose amplitude decreases with decreasing cluster temperature (mass) as $B_* \sim T_{200}^{\eta}$ with $\eta \approx 0.5$ may reproduce, on average, the whole distribution of the data. The best-fit trend of the entropy $S(T)$ evaluated by assuming this phenomenological scaling of the magnetic field amplitude, $B_* \sim T^{0.5}$, is shown in Fig. 8. We also report in Fig. 9 the best-fit relation for the amplitude of the magnetic field, $B_* \propto T_{200}^{0.5}$, plus its variation allowed by the IC gas entropy data.

We notice that the effect of a magnetized IC gas produces an inversion of the entropy at low temperature values, i.e. in the group region, as the one shown by the unbinned data derived from Ponman et al. (2003). Figure 10 shows our best-fit prediction plus the uncertainty region for the $S - T$ relation compared to the unbinned entropy data of Ponman et al. (2003, see their Fig. 4). We also plot in Fig. 11 the $S - M$ relation predicted by our model.

6. The $L_{\rm X} - T$ relation for magnetized clusters

We show in this section that the same physical model that is able to recover the flattening of the $S - T$ relation also provides an explanation for the steepening of the $L_{\rm X} - T$ relation, from the scale of clusters down to the group scale.

Since the X-ray emissivity is mainly provided by thermal bremsstrahlung emission

$$\varepsilon_{\rm brem} \approx 3 \times 10^{-27}\ {\rm erg\ s^{-1}\ cm^{-3}} \rho_{\rm g}^2(r, B) T_{\rm g}^{1/2}(B), \qquad (14)$$

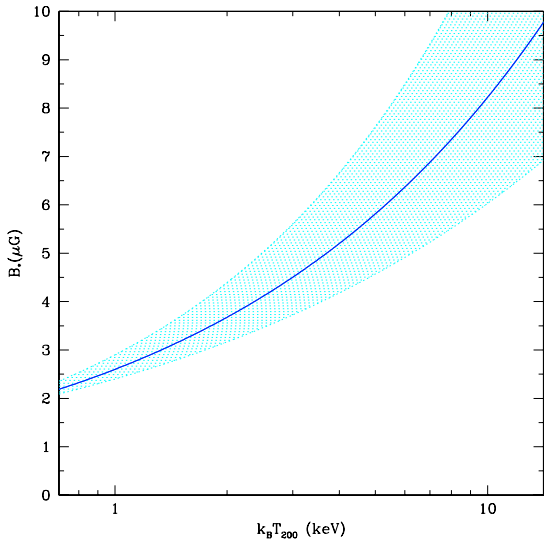

Fig. 9. The function $B_* = 2.6\ \mu\mathrm{G}(T_{200}/\mathrm{keV})^{0.5}$ which best fits the $S - T$ relation in Fig. 8 is shown by the solid curve. The shaded area shows the range of variation of $B_*(T_{200})$ enclosed by the curves $B_* = 2.4\ \mu\mathrm{G}(T_{200}/\mathrm{keV})^{0.4}$ (lower bound) and $B_* = 2.9\ \mu\mathrm{G}(T_{200}/\mathrm{keV})^{0.6}$ (upper bound).

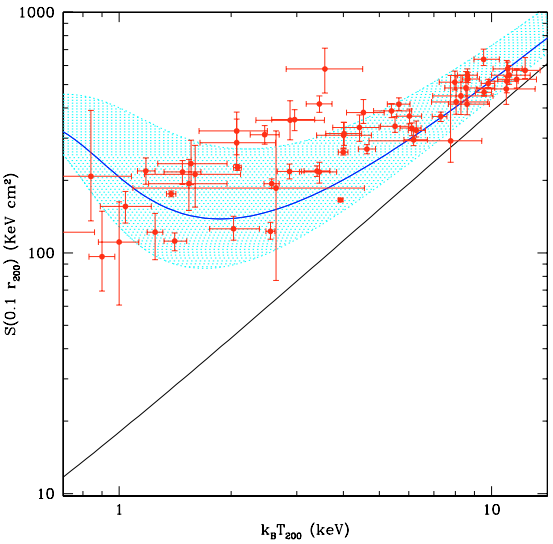

Fig. 10. Same as Fig. 8 but for our best-fit model compared to the unbinned data distribution of Ponman et al. (2003).

(here we adopt its expression for $k_\mathrm{B}T_\mathrm{g} \gtrsim 2$ keV, see Sarazin 1988), the bolometric X-ray luminosity of a cluster with mass M is given by

$$L_\mathrm{X} \propto T_\mathrm{g}^{1/2}(B)\rho_\mathrm{g}^2(0,B)\left(\frac{r_\mathrm{vir}}{c}\right)^3 \int_0^c \mathrm{d}x x^2 y_\mathrm{g}(x,B) \qquad (15)$$

which reads, in practical units, as

$$L_\mathrm{X} \approx 2.8\times10^{45}\ \mathrm{erg\ s^{-1}}\left(\frac{k_\mathrm{B}T_\mathrm{g}(B)}{4\ \mathrm{keV}}\right)^{1/2}\left(\frac{n_\mathrm{g}(0,B)}{10^{-3}\ \mathrm{cm^{-3}}}\right)^2 \times\frac{1}{c^3}\left(\frac{M_\mathrm{vir}}{M_8}\right)\int_0^c \mathrm{d}x x^2 y_\mathrm{g}(x,B). \qquad (16)$$

The presence of a magnetic field provides a strong decrease of the cluster L_X at low temperature due to the decrease of the central IC gas density (see Sect. 2) and also a decrease of the cluster

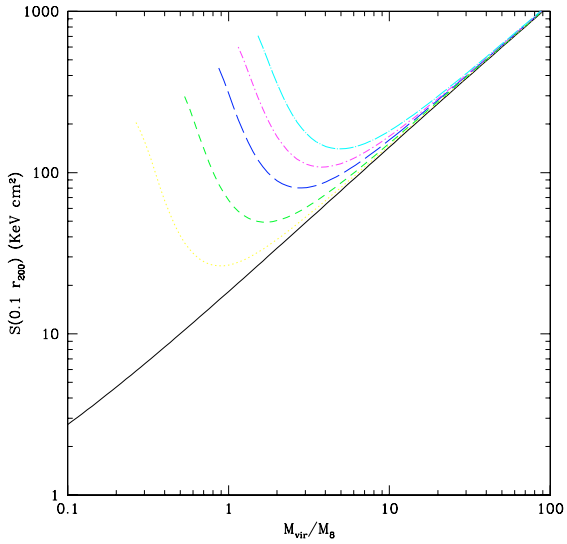

Fig. 11. The entropy $S(0.1r_{200})$ as a function of the cluster virial mass M_vir (in units of M_8) for various values of the magnetic field B_* as in Fig. 7.

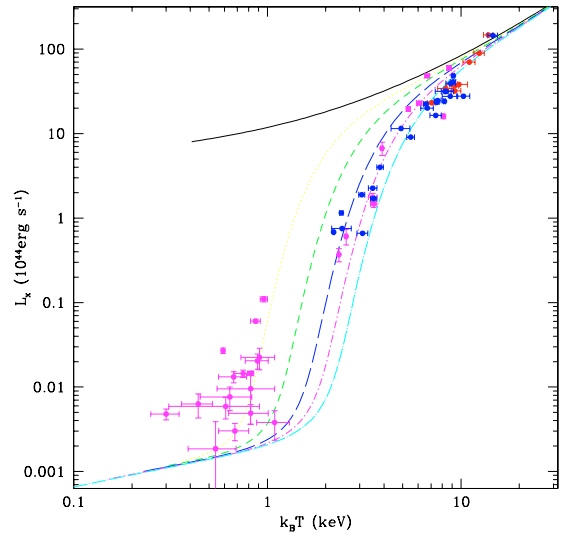

Fig. 12. The bolometric X-ray luminosity L_X as a function of the gas temperature for various values of the magnetic field $B_* = 0$ (black curve), 2.5 μG (yellow), 3.7 μG (green), 5 μG (blue), 6 μG (red) and 7 μG (cyan). Data are taken from Arnaud & Evrard (1999, blue dots), Allen et al. (2001, red dots) and Ponman et al. (2003, magenta dots).

temperature from the MVT with respect to their unmagnetized values.

The result of a simple calculation based on the HE, on the MVT and on the expression of L_X as given in Eqs. (15), (16) is reported in Fig. 12 and it shows that the effect of the magnetic field is to steepen the $L_\mathrm{X} - T$ relation. We stress that the X-ray luminosity data shown in Fig. 12 are enclosed by the same curves that enclose the $S - T$ data in the same temperature range. Moreover, as in the $S - T$ relation, a magnetic field whose amplitude decreases with decreasing cluster mass as $B_* \sim T_\mathrm{g}^{0.5\pm0.1}$ is able to reproduce the whole distribution of the $L_\mathrm{X} - T$ data from groups to clusters. The best-fit trend of the $L_\mathrm{X} - T$ relation evaluated by assuming this phenomenological scaling of the magnetic field amplitude which fits the entropy data (see Figs. 8 and 10) is shown in Fig. 13.

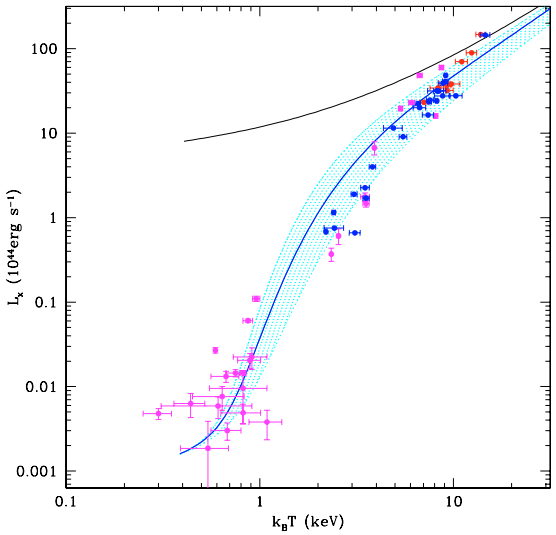

Fig. 13. The bolometric X-ray luminosity L_X as a function of the gas temperature for a magnetic field scaling $B_* \sim T_{200}^{\eta}$ with $\eta = 0.5 \pm 0.1$. Note that this magnetic field scaling is the same that fits the $S - T$ relation, as shown in Fig. 8.

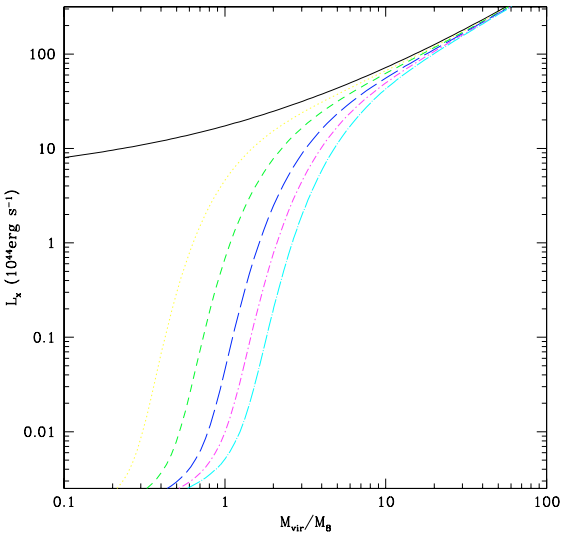

Fig. 14. The bolometric X-ray luminosity L_X as a function of the cluster mass for various values of the magnetic field $B_* = 0$ (black curve), 2.5 μG (yellow), 3.7 μG (green), 5 μG (blue), 6 μG (red) and 7 μG (cyan).

We also show in Fig. 14 the $L_X - M$ relation that is consistent with the $L_X - T$ relation previously discussed.

The fact that the same model for magnetized clusters which is able to reproduce the $S - T$ relation (see Sect. 5) also recovers the $L_X - T$ relation is not a coincidence, but is a consequence of the (reliable) physical description of the X-ray cluster structure. In fact, the entropy $S = T_g/\rho_g^{2/3}$ calculated at a scale $0.1r_{200}$ (i.e., within the cluster core) sets the values of the gas density and temperature at the same spatial scale, and hence the value of the X-ray luminosity $L_X \propto \rho_g^2 T_g$, which is mostly determined by the cluster core properties. Therefore, adjusting the parameters of our model to match the observed $S - T$ relation implicitly ensures that the resulting $L_X - T$ relation is close to the observed one.

7. Exploring the effects of boundary conditions

In the previous sections we have shown the effect of the magnetic field on the $S - T$ and $L_X - T$ relations for the case in which i) the external pressure was negligible (the formal case $P_{ext} = 0$ has been adopted in Sects. 4–6); and ii) the boundary condition used to normalize the IC gas density profile given by Eq. (6), i.e. a constant gas mass within the cluster virial radius.

For completeness, we describe in this section the effects on cluster temperature, entropy and X-ray luminosity induced by changing the previous boundary conditions.

7.1. Normalizing to the cluster virial pressure

Normalizing the IC gas density profile to have a constant pressure at the virial radius, $P_g(r_{vir}, B) = \text{const.}$, yields a decrease of the central gas density with increasing values of B_* which is larger than when normalizing the same density profile to $M_g(r_{vir})$; this happens because, for a given cluster mass (temperature), the former condition requires $\rho_g(r_{vir}, B) = \rho_g(r_{vir}, B = 0)$. This fact implies a behaviour of the function $K(M, B) = \rho_g(r, B)/\rho_g(r, B = 0)$ that is slightly different from that shown in Fig. 2, and consequently a slightly different behaviour of the scaling of $\rho_g(0.1r_{200})$ with the cluster temperature (mass) as shown in Fig. 15. Since the maxima of the function $\rho_g(0.1r_{200})$ are moved to lower temperatures in this case, the inversion of the $S - T$ relation is also moved at lower temperatures and the flattening of the $L_X - T$ relation is found at lower values of the X-ray luminosity and lower temperatures (see Fig. 16). These results show that both the entropy inversion and the flattening of the $L_X - T$ relation at low temperatures are a realistic effect to be expected in models of magnetized clusters; moreover, these results do not strongly depend on the adopted boundary conditions for the gas density profile of the clusters. This reinforces our conclusions on the ability of models of magnetized clusters to reproduce the basic structural properties of X-ray clusters.

To conclude our exploration of the effects of boundary conditions, we will address in the next section the effects on gas density, entropy and X-ray luminosity caused by changing the external pressure P_{ext} at the cluster boundary.

7.2. Changing the cluster external pressure

Changing the value of the external pressure P_{ext} in the MVT modifies the cluster temperature and also alters the solution $\rho_g(r, B)$ of the HE condition as shown in Fig. 17. In fact, increasing the value of P_{ext} yields an increase of the overall cluster temperature (see Eq. (9)) and hence a decrease of the central IC gas density, to be consistent with its boundary conditions (see Fig. 17). The increase of P_{ext} in the MVT and in the HE condition causes a larger decrease of the IC gas density in the cluster core (even in the absence of a magnetic field) and hence a further bending of the temperature dependence of $\rho_g(0.1r_{200})$ in the low-T region than the case in which $P_{ext} = 0$ (see Fig. 6). This behaviour implies that the $S - T$ relation is flatter at low-T with respect to the case in which $P_{ext} = 0$, even for $B_* = 0$ (see Fig. 18). In addition, the entropy inversion which is produced in the low-T region by the effect of magnetic field is further enhanced by the increasing value of P_{ext}. As a direct consequence of this fact, the $L_X - T$ relation computed for values $P_{ext} > 0$ becomes steeper than that derived in the case $P_{ext} = 0$, even in the absence of a magnetic field. The presence of a magnetic field (like the one $B_* \propto T^{0.5}$ that best fits the $S - T$ and the $L_X - T$ relations for $P_{ext} = 0$, see Figs. 8 and 13) further increases the steepness

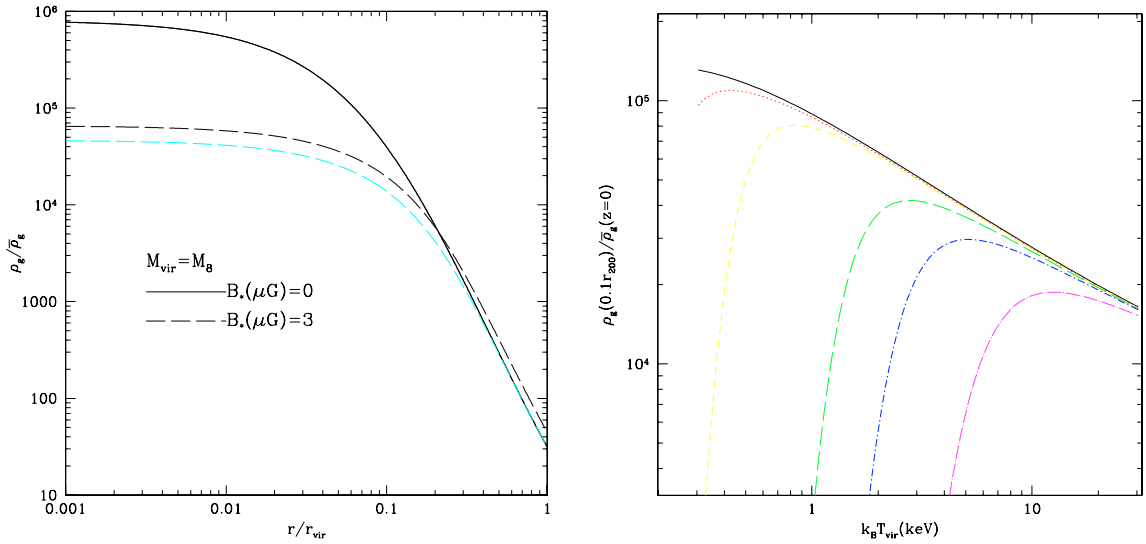

Fig. 15. *Left*. The radial density profiles of the IC gas normalized to the same virial pressure $P_{\rm vir}$ for values of the magnetic field $B_* = 0$ (solid) and $B_* = 3\,\mu$G (dashed cyan) are compared to the analogous density profiles normalized to the total gas mass at $r_{\rm vir}$ (dashed black). A cluster with $M = M_8$ is considered here. *Right*. The temperature dependence of the IC gas density evaluated at $0.1r_{200}$ for the same values of the B-field as in Fig. 6 but for a normalization of the IC gas density to the virial pressure $P_{\rm vir}$.

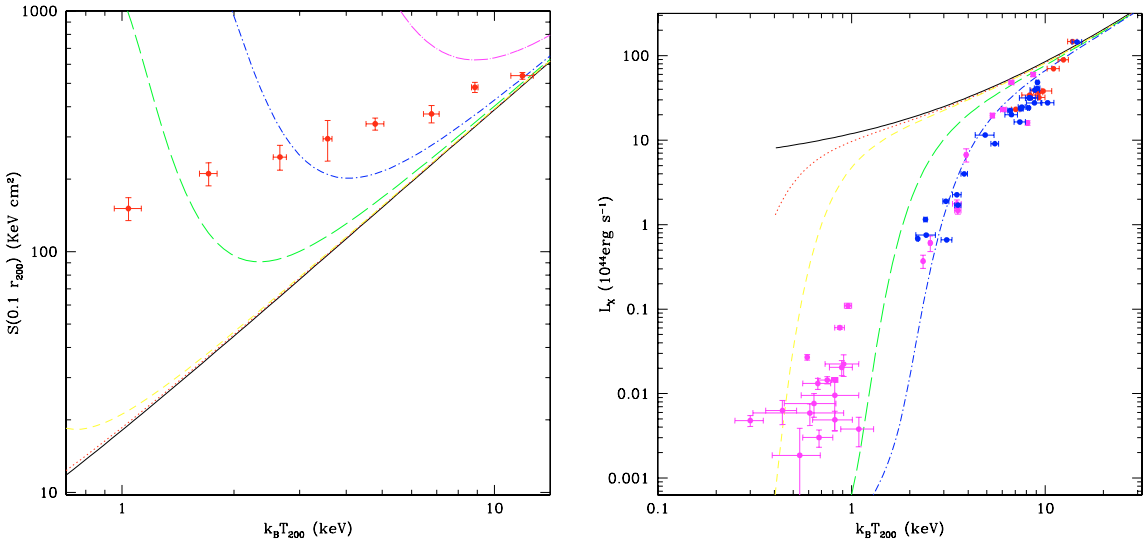

Fig. 16. *Left*. The $S - T$ relation for clusters with IC gas density profiles normalized to the virial pressure $P_{\rm vir}$ is shown for the same values of the magnetic field B_* as in Fig. 7. *Right*. The $L_{\rm X} - T$ relation for clusters with IC gas density profiles normalized to the virial pressure $P_{\rm vir}$ is shown for the same values of the magnetic field B_* as in Fig. 12.

of the predicted $L_{\rm X} - T$ relation towards low temperatures, thus requiring lower values of the magnetic field to reproduce, in this case, the distribution of the available data (see Fig. 18).

Finally, the combination of large values of $P_{\rm ext}$ and a different boundary condition (like the one requiring us to normalize the IC gas density profile to the virial pressure, that we previously explored in this section) has the combined effect of further increasing both the flatness and the inversion of the $S - T$ relation and, consistently, the steepness of the $L_{\rm X} - T$ relation in the low-temperature region (see Fig. 19). We stress that in this last case the $S - T$ and the $L_{\rm X} - T$ relations evaluated for a null magnetic field are no longer representable by simple power-law behaviours, since the presence of a positive external pressure alters the cluster temperature derived from the MVT and the value of $\rho_{\rm g}(0.1r_{200})$. This suggests that, in this case, the observed $L_{\rm X} - T$ relation (as well as the $S - T$ relation) could be roughly reproduced by the combination of high values of $P_{\rm ext}$ with a more modest contribution from the magnetic field (with respect to the case $P_{\rm ext} = 0$), because the effect of $P_{\rm ext}$ in the MVT and in the HE conditions of our model (see Sect. 2) tends to mimic – at a given boundary condition for the IC gas at the cluster virial radius – that of an increasing magnetic field on the IC gas density profile. In fact, the external pressure compresses the IC gas and tends to rise its temperature, thus requiring a decrease of the core density in order to fulfill the IC gas boundary condition at $r_{\rm vir}$. Both the boundary conditions that have been considered here ($M_{\rm g}(r_{\rm vir}) = $ const., or $P_{\rm g}(r_{\rm vir}) = $ const.) provide hence a decrease of the IC gas density in the cluster core which affects both the entropy and the X-ray luminosity, as we have shown here.

By stretching our analysis to the extreme conclusion, we could say that the $S - T$ and the $L_{\rm X} - T$ relations could be reproduced with an appropriate distribution of external pressure values, decreasing from the rich cluster scale down to the group scale, with only a small effect due to the unavoidable presence of

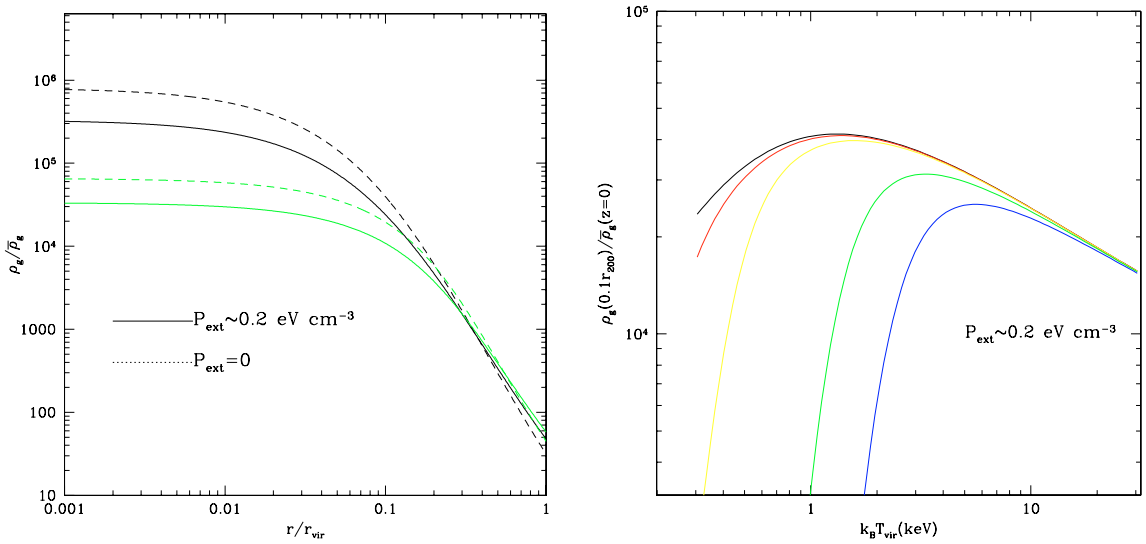

Fig. 17. *Left*. The radial density profiles of the IC gas evaluated in the presence of an external pressure $P_{\rm ext} = 0.2$ eV cm^{-3} (solid curves) are shown for values of $B_* = 0$ (black) and $B_* = 3\,\mu$G (green) and are compared to the analogous profiles evaluated with $P_{\rm ext} = 0$ (dashed curves for the same magnetic field values). A cluster with $M = M_8$ has been chosen. *Right*. The temperature dependence of the IC gas density evaluated at $0.1r_{200}$ is shown for the same values of the B-field as in Fig. 6 but for a value of the external pressure $P_{\rm ext} = 0.2$ eV cm^{-3}.

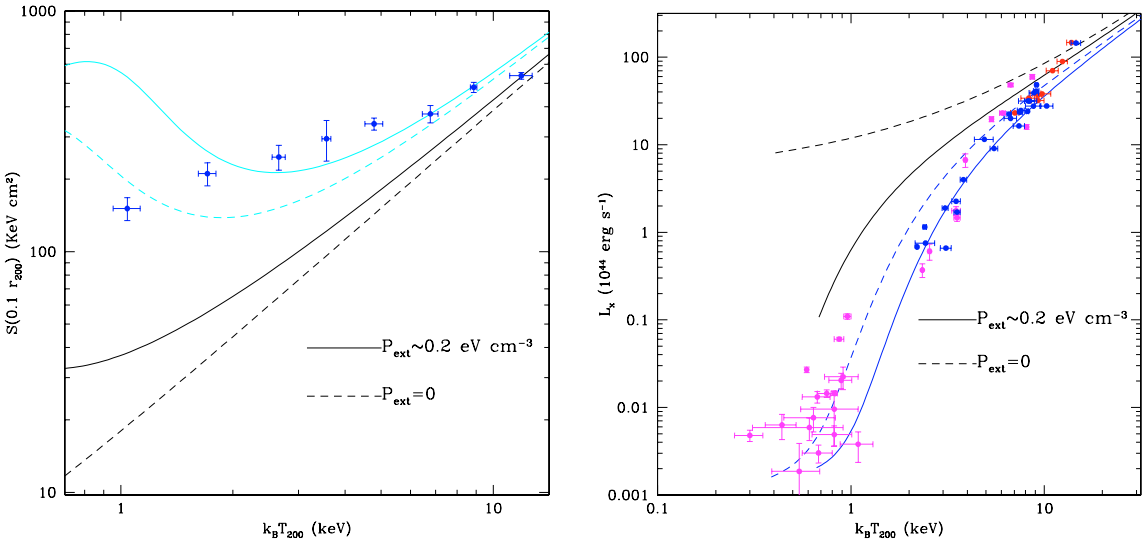

Fig. 18. *Left*. Comparison of the best fit $S - T$ relation evaluated for $P_{\rm ext} = 0$ (dashed cyan, see Fig. 8) and the one calculated for the same parameters but for $P_{\rm ext} = 0.2$ eV cm^{-3} (solid cyan). The $S - T$ relations evaluated in the case $B_* = 0$ with $P_{\rm ext} = 0$ (dashed black) and $B_* = 0$ with $P_{\rm ext} = 0.2$ eV cm^{-3} (solid black) are also shown for comparison. *Right*. The same cases shown for the $S - T$ relation in the left panel of this figure are shown here for the $L_{\rm X} - T$ relation. Different curves refer to the same cases as discussed in the left panel.

a low-amplitude intra-cluster magnetic field. However, we recall that values of $P_{\rm ext} \approx 0.2$ eV cm^{-3} (considered in Figs. 17–19) are found at the outskirts ($r \gtrsim r_{\rm vir}$) of rich, hot clusters (with mean temperatures $\gtrsim$10 keV, see Sect. 2.2) and they are, therefore, extreme values of the external pressure which are much higher than those usually found around low-T clusters and groups. This means that the temperature scaling of the cluster entropy and X-ray luminosity (with and without a magnetic field) for such a high value of $P_{\rm ext}$ considered as representative of the whole population of clusters (from rich ones down to small groups) has to be considered unlikely; a lower value of $P_{\rm ext}$ closer to the value found in the IGM is better suited to the case of low-T systems (see, e.g., our discussion in Sect. 2, see also the results of the temperature and density profile analysis of a sample of poor and rich clusters studied by Piffaretti et al. 2005), and thus the results presented in Sects. 3–6 seem to be more reliable.

The results discussed in this section have been presented for illustrative purposes and are based on a parametric variation of the leading physical quantities and boundary conditions. A more detailed exploration of these effects requires a thorough analysis of the density and temperature profiles of a large sample of groups and rich clusters out to radii $r \gtrsim r_{\rm vir}$, an analysis which is crucial for this issue, but it is not yet available. The previous analysis should be combined with the complementary study of the evolution of the intra-cluster magnetic field with the cluster scale (mass, radius) which has just begun and that will receive a substantial boost from the advent of the next generation radio observatories with high sensitivity and spatial resolution (e.g, SKA, LOFAR). Given the lack of detailed data on these subjects, we will tackle in detail the theoretical aspects related to these issues in a forthcoming paper (Colafrancesco et al. 2007, in preparation).

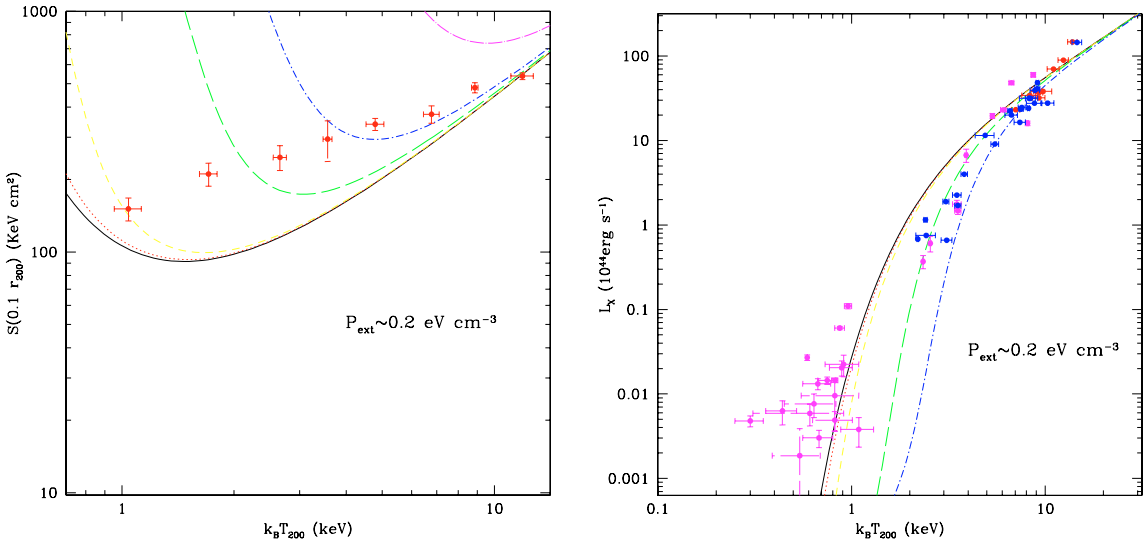

Fig. 19. *Left*. The $S - T$ relation for clusters with IC gas density profiles normalized to the virial pressure $P_{\rm vir}$ and with $P_{\rm ext} = 0.2$ eV cm^{-3}. Curves are for the same values of the magnetic field B_* as in Fig. 7. *Right*. The $L_{\rm X} - T$ relation for clusters with IC gas density profiles normalized to the virial pressure $P_{\rm vir}$ and with $P_{\rm ext} = 0.2$ eV cm^{-3}. Curves are for the same values of the magnetic field B_* as in Fig. 12.

8. Discussion and conclusions

Our results provide an analytical description of the effects of a magnetic field on the density structure and on the entropy profiles of galaxy clusters in the context of the HE condition and of the MVT. We have shown that such a description is able to provide, at once, a possible explanation of three problematic aspects of the cluster structure: i) the flattening of the entropy profile in the cluster center (together with the possible entropy inversion near the center of the structure); ii) the flatness of the $S - T$ relation (together with the entropy inversion at the scale of the galaxy groups); iii) the increasing steepening of the $L_{\rm X} - T$ relation from the cluster scale towards the group scales.

The inclusion of the effects of the magnetic field in the description of the intra-cluster gas structure is motivated by the increasing evidence for the presence of a magnetic field in these cosmic structures (see, e.g., Carilli & Taylor 2002; Govoni & Feretti 2005, for recent reviews).

In the framework of our model, all the available data indicate that an increase of the magnetic field $B_* \sim T^{0.5\pm0.1}$ is able to reproduce, at the same time, both the $S - T$ and the $L_{\rm X} - T$ relations. Such a scaling is a reasonable expectation of hierarchical clustering scenarios in which the magnetic field is coupled to the amount of gas collected in the deepening potential wells of increasing mass systems. The available evidence on the amplitudes of cluster magnetic fields for individual clusters and groups seem to be consistent with this result (see also Cassano et al. 2006, for an independent study).

Since the theoretical results presented here partly depend on the assumed boundary conditions for the IC gas at $r \approx r_{\rm vir}$, we have also provided a systematic exploration of the effects of changing the IC gas boundary conditions on the structure and evolution of X-ray clusters. Such an analysis has been able to show that the study of the magnetic field effects on the IC gas must be addressed in full complementarity with the pressure and density study of the cluster external regions at $r \gtrsim r_{\rm vir}$.

How does the model and the results we have presented here compare to other theoretical explorations of the IC gas physics?

It has been suggested (see, e.g., Arnaud 2005, for a review) that the steepening of the $L_{\rm X} - T$ relation could be due to a systematic change (increase) of the mean gas density with T (i.e., a simple modification of the scaling laws) or to a variation of the cluster shape with T (i.e., a breaking of self-similarity). Many studies have attributed the deviations from self-similarity to an early episode of preheating by supernovae or active galaxies so that the heat input that estabilishes a uniform minimum entropy level in the intergalactic medium breaks the self-similarity because the extra entropy makes the gas harder to compress as it accretes into dark matter halos (e.g., Kaiser 1991; Evrard & Henry 1991). However, several analyses suggested that the energy input required to explain the observed relations through global preheating seems to be quite extreme (see, e.g., Donahue et al. 2006; Arnaud 2005). Alternative explanations (Voit & Bryan 2001) have argued that the entropy scale responsible for the breaking of self-similarity is not a global property of the IGM but rather a condition set by the radiative cooling. In such a scenario, cooling and feedback seem to conspire to deplete the amount of gas below the cooling threshold: thus, some of the low-entropy gas condenses and the feedback subsequently raises the entropy of the remaining gas until both cooling and feedback shut down. Variations on this theme (see, e.g., Voit et al. 2002) are also able to provide models that may account for several X-ray observables (like the $L_{\rm X} - T$ and the $T - M$ relations, the X-ray surface brightness profiles of clusters and their temperature gradient). However, these models are not yet able to explain why clusters differ in the amount of gas that still remains below the cooling threshold.

In such a complex theoretical framework, some recent studies of the self-similarity in the cluster gas temperature and entropy profiles suggest that the departures of the entropy and X-ray luminosity scaling laws from the standard self-similar model could be due to a change in the temperature (mass) dependence of the normalization of the gas density profiles (see Arnaud 2005, for a general discussion).

In our model a non-standard scaling of the IC gas density with the cluster temperature (mass) is provided (see Figs. 1 and 6) by the inclusion of the magnetic field effects on the HE (and the MVT) condition of the IC gas, which then changes both the radial distribution of the IC gas (for a given cluster mass and B-field value) and the relation between the gas temperature and cluster mass. It follows that a consistent description of the

magnetized ICM can provide a simple explanation of several (or of all) of these still open problems and thus weakens the need for the inclusion of non-gravitational effects – like e.g., shock heating, AGN or SN feedback – which have been proposed, so far, for the explanation of these features.

Our study (far from being conclusive) shows that a more global description of the IC gas physics may help in solving some of the crucial aspects of cluster structure and evolution.

In these respects, we want to stress, in the following, some of the limits of this initial study.

The isothermal case that we explored here in detail is not valid for all clusters and groups, even though it seems to be a valid approximation in the intermediate regions of many clusters, from where the entropy data are taken (see, e.g., Pratt et al. 2006; Pointecouteau et al. 2005). Thus, even though our comparison with the entropy data taken from Pratt et al. (2006) and from Ponman et al. (2003) can be quite safe, we need more refined analyses of both the very inner parts (the cool cores at $r \lesssim 0.1 r_{200}$) and the external regions (those at $r \gtrsim r_{200}$) of clusters. The cluster cool cores that show quite high values of the magnetic field, sharp T jumps and probably not isentropic conditions (see, e.g., Piffaretti et al. 2005) and are also sites of complex AGN – IC gas interaction (see, e.g., Fabian 2005), are not considered in a complete self-consistent way here. Our approach to the description of the magnetized IC gas in this region needs a refined analysis of both the MVT and of the HE equation that is beyond the scope of this paper, and will be presented elsewhere. The external regions at $r \gtrsim r_{200}$ usually show a temperature decrease towards the outskirts of the cluster and thus, they also need a further analysis with respect to the isothermal model. The use of a polytropic model (i.e., an extension of our model that we have already worked out in the Appendix) will be also presented elsewhere. The study of the pressure and density structure of the cluster external regions is also relevant to set the appropriate boundary conditions for the IC gas and therefore it requires a more detailed analysis.

Within the limits of its applicability, this first exploration indicates, nonetheless, that a more detailed physical description of the IC gas properties that takes into account also the magnetic field might solve a number of problematic features in cluster structure and evolution.

The predictions of our model can be subject to observational tests. One of the most direct tests is to look for the amplitude of the magnetic field in clusters and groups through FR measurements that could directly prove or disprove the scaling of the magnetic field amplitude $B_* \sim T^{0.5\pm0.1}$ that we predict in order to recover the $S - T$ and $L_X - T$ relations. The few data points available so far seem to be consistent with such a scaling (see also Cassano et al. 2006, for an independent argument). Detailed FR measures in the inner ∼Mpc of groups and clusters will be available in the near future with the forthcoming SKA and LOFAR radio experiments. Some of the cluster will also likely show evidence for extended and diffuse radio emission that will provide further information on the radial distribution of the magnetic field (see, e.g., Colafrancesco et al. 2005, for a more general discussion). Lastly, the combination of high-sensitivity X-ray and radio observations will be able to shed light on the physics of the intra-cluster gas and its associated magnetic field in both the cool cores and in the external regions of clusters at different redshifts, so that it will be possible to determine its detailed physical status as well as its cosmic evolution.

Acknowledgements. We thank the Referee for useful comments that led to improve the presentation and the clarity of our paper. We thank A. Sanderson and T. Ponman for having provided us with the unbinned entropy data for clusters and groups shown in Fig. 10. S.C. acknowledges support by PRIN-MIUR under contract No. 2004027755_003.

Appendix A: The hydrostatic equilibrium equation in the presence of *B*-field

The radial profile of the IC gas density ρ_g can be obtained by solving the hydrostatic equilibrium equation once we specify the equation of state of the gas. In general one writes

$$\nabla p = -\rho_g \nabla \phi(r), \tag{A.1}$$

where p is the sum of all the pressure components in the cluster (IC gas, magnetic field, etc.) and $\phi(r)$ is the gravitational potential. Under the assumption of spherical symmetry and local homogeneity of the gas, Eq. (A.1) writes as

$$\frac{1}{\rho_g}\frac{dp}{dr} = -\frac{d\phi}{dr} = -\frac{GM(r)}{r^2} \tag{A.2}$$

where $M(r)$ is the total mass enclosed in a sphere of radius r. The expression for $M(r)$ depends on the assumed gravitational potential. In the β-profile, one assumes that

$$M(r) = 4\pi\rho_0 r_s^3 \{\ln[x + (1+x^2)^{1/2}] - x(1+x^2)^{-1/2}\}. \tag{A.3}$$

Assuming a NFW universal profile, the mass $M(r)$ writes as

$$M(\le r) = 4\pi\rho_s \left(1 + \frac{\Omega_b}{\Omega_{dm}}\right) r_s^3 m(x), \tag{A.4}$$

where $m(x)$ describes the mass profile of the cluster.

There are various choices for the gas equation of state: (a) the gas follows the Dark Matter, $\rho_g \propto \rho_{dm}$; (b) the cluster is isothermal, T_g = const.; (c) the gas follows a polytropic law, $T_g \propto \rho_g^{\gamma-1}$. In the following we will consider specifically the cases (b) and (c), and we will solve the hydrostatic equilibrium equation for the IC gas density with and without the presence of a magnetic field $B(r)$.

A.1. Isothermal case

Let us consider first the case $B = 0$.

In the case of a NFW mass density profile, Eq. (A.2) can be written as:

$$\frac{k_B T_g}{\mu m_p}\rho_g(r)^{-1}\frac{d\rho_g(r)}{dr} = -\frac{GM(\le r)}{r^2}. \tag{A.5}$$

Since

$$M(\le r) = M_{vir}\left[\frac{m(x)}{m(c)}\right] \tag{A.6}$$

holds, it follows that

$$\frac{dy_g(x)}{y_g(x)} = -\frac{GM_{vir}\mu m_p}{k_B T_g r^2}\left[\frac{m(x)}{m(c)}\right]dr. \tag{A.7}$$

After integration we find

$$\int_0^x \frac{dy_g(x)}{y_g(x)} = -3\frac{T_{vir}}{T_g}\frac{c}{m(c)}\int_0^x \frac{m(u)}{u^2}du, \tag{A.8}$$

$$\int_0^x \frac{dy_g(x)}{y_g(x)} = -3\frac{c}{m(c)}\int_0^x \frac{m(u)}{u^2}du, \tag{A.9}$$

from which

$$\rho_{\rm g}(r) = \rho_{\rm g}(0) {\rm e}^{-3\frac{c}{m(c)}\int_0^x \frac{m(u)}{u^2}{\rm d}u} \tag{A.10}$$

obtains. The quantity $T_{\rm vir} = \frac{GM_{\rm vir}\mu m_{\rm p}}{3k_{\rm B}r_{\rm vir}}$ is the virial temperature and $\rho_{\rm g}(0)$ is the central gas density.

When $B \neq 0$, the hydrostatic equilibrium condition (Eq. (A.2)) is modified since an additional magnetic pressure term exists:

$$\frac{\partial p_{\rm g}(r,B)}{\partial r} + \frac{\partial p_B(r,B)}{\partial r} = -\frac{GM(\leq r)}{r^2}\rho_{\rm g}(r,B), \tag{A.11}$$

where

$$B(r) \propto B_*(\mu G)\rho_{\rm g}(r,B)^{\alpha} \tag{A.12}$$

and

$$p_B \propto B^2. \tag{A.13}$$

The HE condition in Eq. (A.11) can be written as:

$$\rho_{\rm g}(r,B)^{-1}C_1\frac{\partial\rho_{\rm g}(r,B)}{\partial r} + \frac{C_2^2}{8\pi}\rho_{\rm g}(r,B)^{-1} \times\frac{\partial\rho_{\rm g}(r,B)^{2\alpha}}{\partial r} = -\frac{GM(\leq r)}{r^2} \tag{A.14}$$

and

$$\rho_{\rm g}(r,B)^{-1}C_1\frac{\partial\rho_{\rm g}(r,B)}{\partial r} + \frac{C_2^2}{8\pi} \quad \rho_{\rm g}(r,B)^{-1}\left(\frac{2\alpha}{2\alpha-1}\right) \times\rho_{\rm g}(r,B)\frac{\partial\rho_{\rm g}(r,B)^{2\alpha-1}}{\partial r} = -\frac{GM(\leq r)}{r^2}, \tag{A.15}$$

where $C_1 = p_{\rm g}(0,B)/\rho_{\rm g}(0,B) \propto k_{\rm B}T_{\rm g}$ and $C_2 = B_*(10^4\bar{\rho}_{\rm g}(z=0))^{-\alpha}$. It follows that

$$y_{\rm g}(x,B)^{-1}\frac{\partial y_{\rm g}(x,B)}{\partial r} + \left(\frac{2\alpha}{2\alpha-1}\right)C_1^{-1}\frac{C_2^2}{8\pi}\frac{\partial y_{\rm g}(r,B)^{2\alpha-1}}{\partial r} = -C_1^{-1}\frac{GM(\leq r)}{r^2}\cdot \tag{A.16}$$

After some algebra, the following equation

$$\frac{{\rm d}y_{\rm g}(x,B)}{y_{\rm g}(x,B)} + \frac{\rho_{\rm g}(0,B)^{2\alpha}}{p_{\rm g}(0,B)}\left(\frac{2\alpha}{2\alpha-1}\right)\frac{C_2^2}{8\pi}{\rm d}y_{\rm g}(x,B)^{2\alpha-1} = -\frac{\rho_{\rm g}(0,B)}{p_{\rm g}(0,B)}\frac{GM(\leq r)}{r^2}{\rm d}r \tag{A.17}$$

is found, and after integration one obtains:

$$\ln y_{\rm g}(r,B) + \eta'(y_{\rm g}(r,B)^{2\alpha-1}-1) = \frac{\ln y_{\rm g}(r,0)}{1-\frac{M_\phi(B)^2}{M_{\rm vir}^2}+\frac{4\pi}{G}\frac{r_{\rm vir}^4}{M_{\rm vir}^2}P_{\rm ext}}, \tag{A.18}$$

$$\eta' = \frac{C_2^2}{8\pi}\left(\frac{2\alpha}{2\alpha-1}\right)\rho_{\rm g}(0,B)^{2\alpha-1}\frac{\mu m_{\rm p}}{k_{\rm B}T_{\rm g}(B)}, \tag{A.19}$$

where $y_{\rm g}(r,0)$ is defined by equation Eq. (A.10). The solution of this equation provides the radial profile of the gas density once the constants $\rho_{\rm g}(0,B)$ and $T_{\rm g}(B)$ are known. The central gas density is set as

$$\rho_{\rm g}(0,B) = \rho_{\rm g}(0,0), \tag{A.20}$$

while the temperature

$$T_{\rm g}(B) = T_{\rm g}(0)\left(1-\frac{M_\phi(B)^2}{M_{\rm vir}^2}+\frac{4\pi}{G}\frac{r_{\rm vir}^4}{M_{\rm vir}^2}P_{\rm ext}\right) \tag{A.21}$$

is obtained from the MVT (see Colafrancesco & Giordano 2006, for a derivation). For a given cluster gas mass, the density profile should be re-normalized as

$$M_{\rm g,vir}(B) = M_{\rm g,vir}(B=0) \tag{A.22}$$

from which the condition

$$\rho_{\rm g}(B,0) = \rho_{\rm g}(0,0)\frac{\int{\rm d}x x^2 y_{\rm g}(x,0)}{\int{\rm d}x x^2 y_{\rm g}(x,B)} \tag{A.23}$$

obtains.

A.2. Polytropic case

Let us consider first the case $B = 0$.

Assuming

$$p_{\rm g} \propto \rho_{\rm g}^{\gamma}, \tag{A.24}$$

Eq. (A.2) writes as:

$$K_1\rho_{\rm g}(r)^{-1}\frac{{\rm d}\rho_{\rm g}(r)^{\gamma}}{{\rm d}r} = -\frac{GM(\leq r)}{r^2}, \tag{A.25}$$

with $K_1 = p_{\rm g}(0)/\rho_{\rm g}(0)^{\gamma}$. From this one obtains

$$K_1\frac{\gamma}{\gamma-1}\rho_{\rm g}(0)^{\gamma-1}\frac{{\rm d}y_{\rm g}(r)^{\gamma-1}}{{\rm d}r} = -\frac{GM(\leq r)}{r^2}, \tag{A.26}$$

and

$$\frac{{\rm d}y_{\rm g}(r)^{\gamma-1}}{{\rm d}r} = -\left(\frac{\gamma-1}{\gamma}\right)\frac{GM(\leq r)\mu m_{\rm p}}{k_{\rm B}T_{\rm g}(0)r^2}\cdot \tag{A.27}$$

From Eq. (A.6) and after integration between the limits $r = 0$ and r, one finds the profile

$$\rho_{\rm g}(r) = \rho_{\rm g}(0) \times\left[1-3\frac{T_{\rm vir}}{T_{\rm g}(0)}\left(\frac{\gamma-1}{\gamma}\right)\frac{c}{m(c)}\int_0^x\frac{m(u)}{u^2}{\rm d}u\right]^{\frac{1}{\gamma-1}}, \tag{A.28}$$

with

$$\frac{T_{\rm g}(0)}{T_{\rm vir}} = \frac{3}{\gamma}\frac{c}{m(c)}|S_*|^{-1} \times\left(\frac{m(c)}{c}+(\gamma-1)|S_*|\int_0^c\frac{m(u)}{u^2}{\rm d}u\right) \tag{A.29}$$

$$\gamma = 1.15 + 0.01(c-6.5), \tag{A.30}$$

and $S_* \equiv {\rm d}\ln y_{\rm dm}(x)/{\rm d}\ln x|_c$.

For $B \neq 0$, Eq. (A.11) is substituted by the following equation:

$$K_1\rho_{\rm g}(r,B)^{-1}\frac{\partial\rho_{\rm g}(r,B)^{\gamma}}{\partial r} + \frac{K_2^2}{8\pi}\rho_{\rm g}(r,B)^{-1} \times\frac{\partial\rho_{\rm g}(r,B)^{2\alpha}}{\partial r} = -\frac{GM(\leq r)}{r^2}, \tag{A.31}$$

and

$$\left(\frac{\gamma}{\gamma-1}\right)\frac{\partial\rho_{\rm g}(r,B)^{\gamma-1}}{\partial r}+K_1^{-1}\frac{K_2^2}{8\pi}\left(\frac{2\alpha}{2\alpha-1}\right)\times\frac{\partial\rho_{\rm g}(r,B)^{2\alpha-1}}{\partial r}=-K_1^{-1}\frac{GM(\leq r)}{r^2} \quad (A.32)$$

with $K_2 \equiv C_2$. Then, it follows

$$\frac{\partial y_{\rm g}(r,B)^{\gamma-1}}{\partial r}+\left(\frac{\gamma-1}{\gamma}\right)\left(\frac{2\alpha}{2\alpha-1}\right)\frac{K_2^2}{8\pi}\frac{\rho_{\rm g}(0,B)^{2\alpha}}{p_{\rm g}(0,B)}\times\frac{\partial y_{\rm g}(r,B)^{2\alpha-1}}{\partial r}=-\left(\frac{\gamma-1}{\gamma}\right)\frac{\rho_{\rm g}(0,B)}{p_{\rm g}(0,B)}\frac{GM(\leq r)}{r^2}. \quad (A.33)$$

After integration one finds

$$y_{\rm g}^{\gamma-1}(x,B)+\eta y_{\rm g}^{2\alpha-1}(x,B)=(1+\eta)y_{\rm g}^{\gamma-1}(x,B=0), \quad (A.34)$$

where

$$\eta=\frac{p_B(r=0,B)}{p_{\rm g}(r=0,B)}\frac{2\alpha}{2\alpha-1}\frac{\gamma-1}{\gamma}. \quad (A.35)$$

To also solve numerically Eq. (A.34) we have to know the quantities γ, $T_{\rm g}(0,B)$ and $\rho_{\rm g}(0,B)$. The quantity γ is independent of the magnetic field $\boldsymbol{B}$; the quantities $T_{\rm g}(0,B)$ and $\rho_{\rm g}(0,B)$ are related to the corresponding quantities for $B=0$ by the relations:

$$T_{\rm g}(0,B)=\frac{T_{\rm g}(0,0)}{1+\eta}, \quad (A.36)$$

As a consequence, it follows that:

$$\rho_{\rm g}(0,B)=\frac{\rho_{\rm g}(0,0)}{(1+\eta)^{\frac{1}{1-\gamma}}}. \quad (A.37)$$

References

Arnaud, M. 2005, in Background Microwave Radiation and Intracluster Cosmology, ed. F. Melchiorri, & Y. Rephaeli (IOS Press, The Netherlands, and Societá Italiana di Fisica, Bologna, Italy), 77 [arXiv:astro-ph/0508159]

Arnaud, M., & Evrard, A. 1999, MNRAS, 305, 631

Arnaud, M., Pointecouteau, E., & Pratt, G. W. 2005, A&A, 441, 893

Carilli, C. L., & Taylor, G. B. 2002, ARA&A, 40, 319

Cassano, R., Brunetti, G., & Setti, G. 2006 [arXiv:astro-ph/0604103]

Colafrancesco, S., Dar, A., & De Rujula, A. 2004, A&A, 413, 441

Colafrancesco, S., Marchegiani, P., & Perola, G. C. 2005, A&A, 443, 1

Colafrancesco, S., & Giordano, F. 2006, A&A, 454, L131

Colafrancesco, S., & Giordano, F. 2007, A&A, submitted

Colafrancesco, S., Profumo, S., & Ullio, P. 2006, A&A, 455, 21

Dolag, K., Bartelmann, M., & Lesch, H. 2002, A&A, 387, 383

Donahue, et al. 2006, ApJ, 643, 730

Eke, V., Cole, S., Frenk, C. S., et al. 1996, MNRAS, 282, 263

Evrard, A. G., & Henry, P. 1991, ApJ, 383, 95

Evrard, A. G., Metzler, C. A., & Navarro, J. F. 1996, ApJ, 469, 494

Fabian, A. C. 2005, Phil. Trans. Roy. Soc. Lond. A, 363, 725 [arXiv:astro-ph/0407484]

Fang, T., & Bryan, G. L. 2001, ApJ, 561, L31

Fujita, Y., Takizawa, M., & Sarazin, C. L. 2003, ApJ, 584, 190

Giovannini, M. 2004, Int. J. Mod. Phys. D, 13, 391

Kaiser, N. 1991, ApJ, 383, 104

Komatsu, E., & Seljak, U. 2001, MNRAS, 327, 1353

Makino, N., Sasaki, S., & Suto, Y. 1998, ApJ, 497, 555

Markevitch, M. 1998, ApJ, 504, 27

Mohr, J. J., Mathiesen, B., Evrard, A. E., et al. 1999, ApJ, 517, 627

Mushotzky, R. F. 2003 [arXiv:astro-ph/0311105]

Navarro, J., Frenk, C., & White, S. D. M. 1997, ApJ, 490, 493

Piffaretti, R., Jetzer, P., Kaastra, J., & Tamura, T. 2005, A&A, 433, 101

Ponman, T., Cannon, D. B., Navarro, J. F., et al. 1999, Nature, 397, 135

Ponman, T., Sanderson, A. J. R., Finoguenov, A., et al. 2003, MNRAS, 343, 331

Pointecouteau, E., Arnaud, M., & Pratt, G. W. 2005, A&A, 435, 1

Pratt, G., & Arnaud, M. 2003, A&A, 408, 1

Pratt, G. W., Arnaud, M., & Pointecouteau, E. 2006, A&A, 446, 429

Rasia, E., Ettori, S., Moscardini, L., et al. 2006, MNRAS, 369, 2013

Ryu, D., Kang, H., Hallman, E., & Jones, T. W. 2003, ApJ, 593, 599

Sarazin, C. L. 1988, X-Ray Emission from Clusters of Galaxies (Cambridge: Cambridge University Press)

Seljak, U. 2000, MNRAS, 318, 203

Voit, M. 2005, AdSpR, 36, 701

Voit, M., & Bryan, G. L. 2001, Nature, 414, 425

Voit, M., Bryan, G. L., Balogh, M. L., & Bower, R. G. 2002, ApJ, 576, 601

Wu, X.-P., & Xue, Y.-J. 2002, ApJ, 572, 19

Zhang, P. 2003, MNRAS, 348, 1348